Theoretical framework for predicting inorganic fouling in membrane distillation and experimental validation with calcium sulfate

Theoretical framework for predicting inorganic fouling in membrane distillation and experimental validation with calcium sulfate[1]

David M. Warsinger, Emily W. Tow, Jaichander Swaminathan, John H. Lienhard V*,

Rohsenow Kendall Heat Transfer Laboratory, Department of Mechanical Engineering

Massachusetts Institute of Technology, 77 Massachusetts Avenue, Cambridge MA 02139-4307 USA

*Corresponding Author lienhard@mit.edu

Abstract

A methodology for predicting scaling in membrane distillation (MD), which considers thermodynamics, kinetics, and fluid mechanics, is developed and experimentally validated with calcium sulfate. The theory predicts the incidence of scaling as a function of temperature, concentration, and flow conditions by comparing the nucleation induction time to the residence time and applying an experimental correction factor. The relevant residence time is identified by considering a volume of solution near the membrane surface that contains enough ions to form a nucleus of critical size. The theory is validated with fouling experiments using calcium sulfate as a model scalant over a range of temperatures (40-70°C), saturation indices, and flow rates. Although the model is validated with a bench-scale MD system, it is hoped to be compatible with large-scale systems that may have significant changes in concentration, temperature, and flow rate along the flow direction. At lower temperatures, the saturation index can be as high as 0.4-0.5 without scaling, but the safe concentration limit decreases with increasing temperature. Increasing the feed flow rate reduces concentration polarization and fluid residence time, both of which decrease the likelihood of fouling. The model is translated into easily readable maps outlining safe operating regimes. The theory and maps can be used to define the safe operating regime in MD over a wide range of conditions and system geometries.

---

[1] Citation: D.M. Warsinger, E.W. Tow, J. Swaminathan, and J.H. Lienhard V, "Theoretical framework for predicting inorganic fouling in membrane distillation and experimental validation with calcium sulfate," *J. Membrane Sci.*, online 22 Jan. 2017, **528**:381-390, 15 April 2017. (doi link) (free download)

Keywords

membrane distillation; fouling; calcium sulfate; nucleation; induction time.

Graphical Abstract

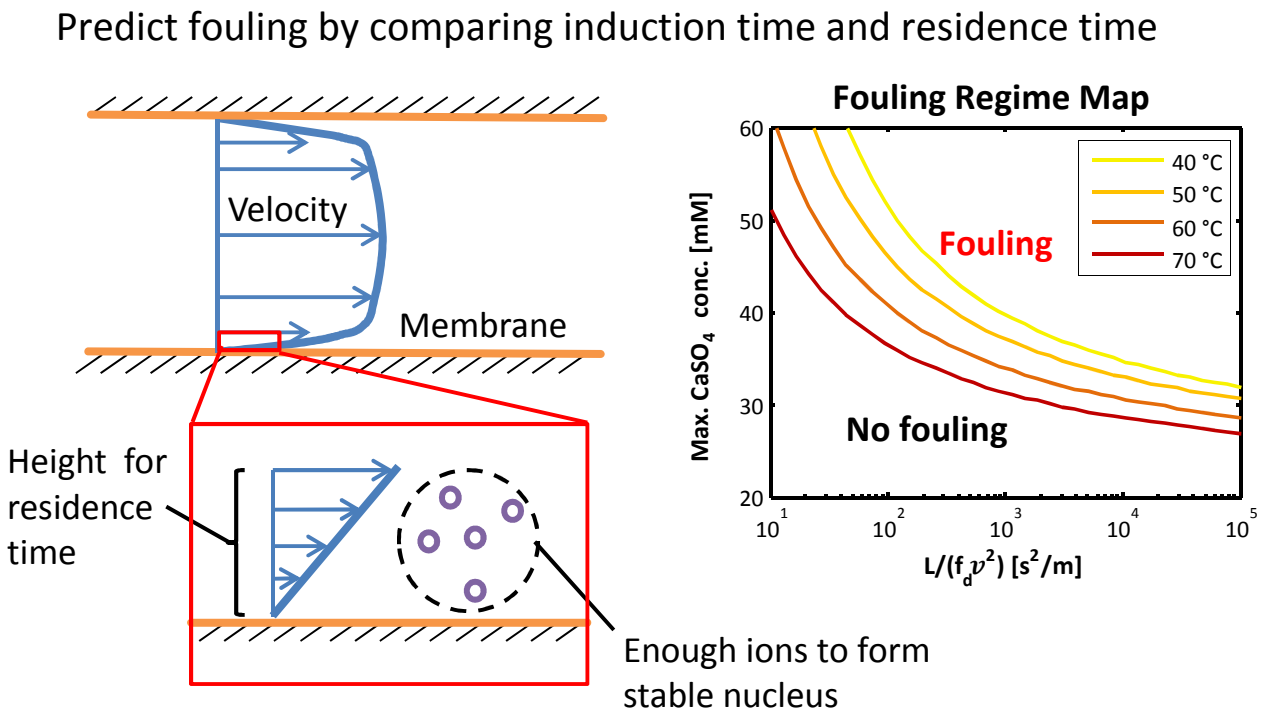

Nomenclature

$a_{\pm}$	Mean ionic activity [-]
$a_{\pm,sat}$	Mean ionic activity at saturation [-]
b, c	Constants fit from nucleation time data [-]
C	Concentration of calcium sulfate at membrane [mol/m^3]
C_{sat}	Saturation concentration of calcium sulfate [mol/m^3]
D_h	Hydraulic diameter [m]
f_d	Darcy friction factor [-]
ΔG_V	Volumetric Gibbs energy change [J/m^3]
L	Membrane length [m]
M_w	Solute molar mass [kg/mol]
N_A	Avogadro constant [mol^{-1}]
n_{min}	Minimum number of molecules in a stable nucleus [-]
P	Pressure [Pa]
R	Universal gas constant [J/mol-K]
r_c	Critical radius [m]
Re_{Dh}	Feed channel Reynolds number = $2\rho_l v h/\mu_l$ [-]
SI	Saturation index [-]
t_{res}	Residence time [s]
t_{res}*	Relevant residence time for fouling prediction [s]
u	Local velocity [m/s]
v	Average velocity [m/s]
V	Volume [m^3]
z	Distance from membrane [m]
z_{min}	Distance from membrane containing enough ions to form a critical nucleus [m]
γ	Interfacial energy of crystal in saturated solution [J/m^2]
μ_l	Liquid dynamic viscosity [Pa-s]
ρ_l	Liquid density [kg/m^3]
ρ_x	Scalant crystal density [kg/m^3]
φ	Experimental fitting parameter [-]

1. Introduction

Membrane distillation is a desalination technology thought to have relatively high fouling resistance in comparison to other membrane-based desalination technologies such as reverse osmosis (RO) [1]. MD relies on evaporation of water from a hot saline feed through a hydrophobic, porous membrane that allows the passage of vapor but not liquid water [2, 3]. The fouling and scaling resistance of MD makes it a promising technology for high salinity applications. MD is especially promising where high osmotic pressure precludes the use of conventional RO, such as in zero liquid discharge systems and for some mining and industrial water treatment [4]. However, the cause of fouling resistance in MD is poorly understood. The literature offers many experimental studies but little fundamental explanation [5]; however, the hydrophobicity of the membrane is thought to minimize surface crystallization [6]. A fundamental understanding of MD fouling is needed, as is a practical approach to predicting the fouling limits of MD with complex solutions.

Previous studies have shown that MD can withstand significantly supersaturated conditions, and that filtration and membrane superhydrophobicity are the most effective existing methods to enhance the fouling resistance of MD [5, 7]. Numerous pilot studies have found good resistance to fouling, but have documented significant flux decline and membrane wetting when fouling did occur [8, 9, 10]. The inorganic salts most likely to cause scaling in many cases are calcium sulfate and calcium carbonate [11], which are the found in seawater, groundwater, and mining applications. Resounding evidence shows that filters are extremely effective in reducing fouling-related flux decline [12, 13, 14, 15] and directly observable fouling [5, 16, 17]. Several past studies [7] have found that crystals were only observed when the membrane dried out, not in-situ during normal operation [7, 18]. This is evidenced by the absence of crystals when the system was allowed to drain, even under very saline conditions (e.g., saturation index (SI) between 1.08 and 1.93 on strongly hydrophobic membranes [7]). When fouled membranes that had flux decline during operation have been examined, the observed crystals are sparsely scattered over the membrane surface, with many areas remaining free of crystals [6].

Understanding the effect of surface properties on crystal nucleation is necessary for scaling prediction. As detailed by Warsinger et al. [19], the Gibbs energy barrier for heterogeneous nucleation on a surface can be expressed as a function of surface energies between the liquid, crystal, and

substrate [20, 21]. This energy barrier influences the nucleation induction time, which is the delay before observable nucleation occurs [21]. These surface energies dictate the contact angle on the surface, thus linking hydrophobicity to induction time at the surface [19]. However, past work has shown that crystal nucleation in membrane distillation occurs largely in the bulk feed solution [6], rather than beginning on the membrane surface as in RO [11]. This difference results from the low surface energy of MD membranes, which are hydrophobic, in contrast to the high surface energy [22] of (hydrophilic) RO membranes [19].

Modeling scaling in MD is complex because of the fluid flow and gradients in temperature and concentration. While classical nucleation theory has focused on induction time in stagnant, heterogeneous solutions, this time can be compared to the fluid maximum residence time within a region of interest to determine whether bulk nucleation will occur. In the present work, we develop theory based on comparison of induction time and residence time, and we validate the theory with multi-day MD fouling experiments using calcium sulfate. From these results, we create a regime map in terms of temperature, saturation index, flow rate, and channel geometry that outlines safe regimes for fouling-free operation, which is readily usable by industry practitioners (section 4.4).

2. Theory Development

Fouling can be approached from one of two standpoints: an Eulerian one, in which induction time theory suggests that crystallization at a given location will occur eventually for almost any supersaturated feed, and a Lagrangian approach that follows the solutes, recognizing that they may move through the membrane module without having time to crystallize. In previous induction time experiments [23, 24, 25], the supersaturated solution is in a closed system, and a model for conditions in a moving fluid was not needed.

Here, we take the Lagrangian approach, and we postulate that fouling will occur when the fluid residence time in the channel exceeds the nucleation time for any precipitate. However, evaluating the exact onset of fouling is not straightforward because both induction time and residence time vary within the channel. The highest residence times occur in the slow-moving boundary layer near the membrane surface (Fig. 1) and vary with distance from the wall.

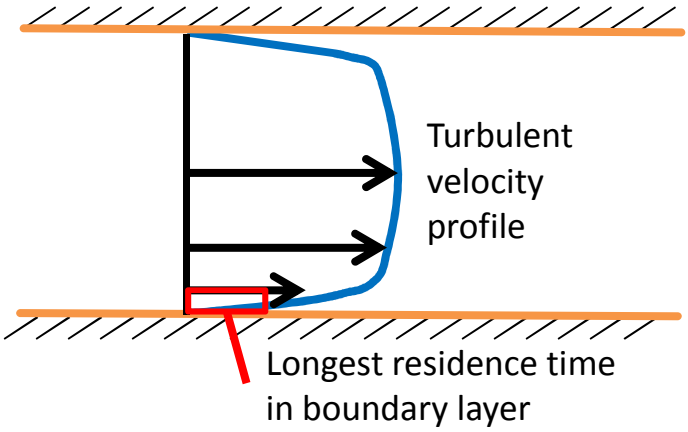

Figure 1. The maximum residence time in the system occurs in the boundary layer near the membrane.

2.1 Residence Time

Near the channel wall, in the boundary layer, the velocity approaches zero and the residence time (inversely proportional to the velocity) of a fluid parcel in the channel approaches infinity. However, very close to the channel wall, there are not enough ions to form a stable nucleus of a critical radius. We postulate that a group of ions large enough to form a critical nucleus must all be in residence long enough to allow for nucleation [26]. The number of molecules needed to form a critical nucleus of radius r_c is n_{min}:

$$n_{min} = \frac{V_{crit}}{V_{molecule}} = \frac{\frac{4}{3}\pi r_c^3}{\frac{M_W}{N_A \rho_x}} \quad (1)$$

where V_{crit} is the volume of a critical nucleus, $V_{molecule}$ is the average volume of a salt molecule in solid form, M_w is the molar mass, N_A is the Avogadro constant, and ρ_x is the crystal density. The need for a critical nucleus for crystal growth arises from the high surface free energy per unit volume of small particles, as discussed in [23].

We assume that the relevant distance z from the channel wall (i.e., the membrane) is very small compared to the thickness of the channel, so that the properties of the fluid (e.g., temperature, concentration) can be considered uniform in the nucleation region and equal to the value at the wall (z=0). A sphere of fluid containing n_{min} molecules in excess of the number that would be present at saturation has a diameter of z_{min}:

$$z_{min} = 2r_c \left(\frac{\rho_x}{M_w\,(C - C_{sat})}\right)^{1/3} \quad (2)$$

where C is the concentration near the wall of the crystal-forming molecule in moles per cubic meter and C_{sat} is the saturation concentration at the local temperature. The distance z_{min} from the wall is shown in Fig. 2.

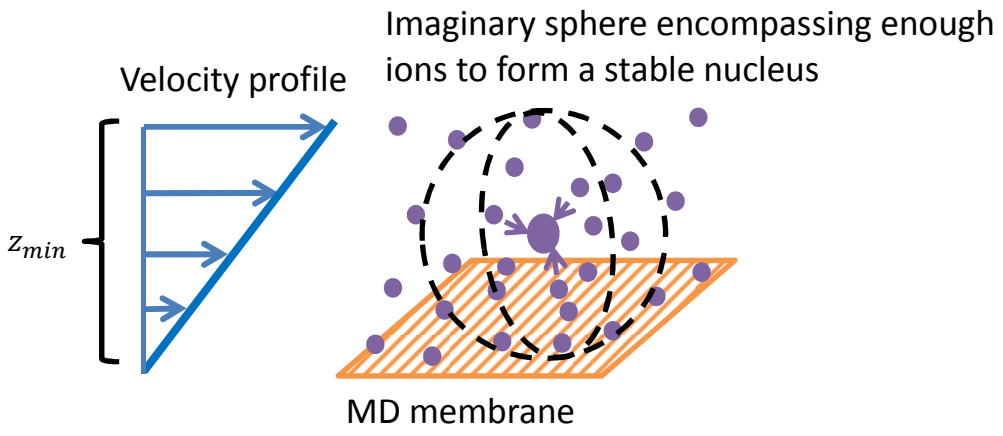

Figure 2. The flow profile and distance z_{min} can be used to calculate the residence time. z_{min} is the distance from the wall that encompasses enough ions to form a stable nucleus.

Because enough ions are present locally to form a critical nucleus within a distance of z_{min} from the wall, z_{min} is the distance from the wall at which the residence time (based on the local velocity) will be compared to the nucleation time. The residence time at z_{min} can be computed using existing correlations for Darcy friction factor f_d, neglecting any effects of the solvent flux on friction factor due to the high ratio of tangential to normal velocity (order 10^5). The pressure drop calculated with the Darcy friction factor can be equated to that calculated from a force balance considering viscous drag on the channel walls:

$$\Delta P = f_d \frac{L}{h}\frac{\rho_l v^2}{4} = \frac{2L\mu_l}{h}\left.\frac{du}{dz}\right|_{z=0}, \quad (3)$$

where ΔP is the pressure drop through a channel of length L, ρ_l is the liquid density, v is the bulk velocity of the flow in the channel, μ_l is the liquid dynamic viscosity, and u is the local mean velocity tangential to the membrane.

Solving the above for the velocity gradient at the wall and assuming that, if the flow is turbulent, z_{min} lies within the viscous sublayer, the local velocity profile is linear and the velocity at z_{min} can be related to f_d:

$$u(z_{min}) = \left.\frac{du}{dz}\right|_{z=0} z_{min} = \frac{z_{min} f_d \rho_l v^2}{8\mu_l}. \quad (4)$$

For the range of conditions experimentally tested in Sec. 4.3 for calcium sulfate, z_{min} is on the scale of 100 nm, and thus is well within the viscous sublayer for typical flows in MD.

Solving for the residence time at z_{min} and incorporating Equations (2) and (4) leads to an expression for the relevant residence time for crystal formation, t^*_{res}:

$$t^*_{res} = t_{res}(z_{\min}) = \frac{L}{u(z_{min})} = \frac{4\mu_l L}{f_d \rho_l v^2 r_c}\left(\frac{M_w\,(C - C_{sat})}{\rho_x}\right)^{1/3}. \quad (5)$$

The relevant residence time for gypsum fouling, t^*_{res}, is on the order of 1000 times higher than the residence time of the bulk fluid, v/L.

The criterion for fouling is met if the induction time is less than the relevant residence time, or:

$$t_{ind} < \varphi\, t^*_{res}, \quad (6)$$

where φ is an experimental fitting parameter intended to account for approximations made in this model and the discrepancy between measured induction time and nucleation time.

To evaluate the fouling criterion, the friction factor, concentration, critical radius, and induction time are needed. Friction factor can be determined from the Reynolds number, $\mathrm{Re}_{Dh,}$ evaluated at the hydraulic diameter, $D_h = 2h$. For turbulent flows, the friction factor f_d is calculated from the Colebrook-White correlation for smooth pipes, which extends to rectangular ducts [27]:

$${f_d}^{-1/2} = 2.0\,\log_{10}\left(\mathrm{Re}_{D_h}\,{f_d}^{1/2}\right) - 0.8. \quad (7)$$

For fully developed laminar flow in the feed channel, the friction factor for flow between parallel plates is given by

$$f_d = 96/\mathrm{Re}_{D_h}. \quad (8)$$

The turbulent friction factor correlation used assumes hydrodynamically smooth walls, which requires that the surface roughness be substantially less than the viscous sublayer thickness [28]. Using the $1/7^{th}$ power law model for the turbulent flow profile [27], the viscous sublayer thickness was calculated

to be about 500 µm for the conditions of the experiments in this study. In comparison, the roughness of the MD membrane was of similar order to that of the pore size, about 0.2 µm [6]. According to the Haaland correlation, friction factor is unaffected by roughness when the ratio of roughness to diameter is much less than $21.1\mathrm{Re}_d^{0.901}$, which is the case for the range of Reynolds numbers considered here [27]. Nuclei are even smaller than the surface roughness, so they should also not impact the friction factor. Although subsequent crystal growth may influence the friction factor, the present model only addresses the onset of fouling, and modeling flow after fouling is outside the scope of this study.

The relevant residence time depends on the critical radius for nucleation. The critical radius r_c is estimated assuming a spherical nucleus as a function of the volumetric Gibbs energy change ΔG_V associated with crystallization and the surface energy γ of the crystal–solution interface via the nucleation equation:

$$r_c = -\frac{2\gamma}{\Delta G_V} \ . \qquad (9)$$

Although the nucleus will not be truly spherical, the value for interfacial energy used here is based on a semi-empirical nucleation induction time expression that includes a geometric factor [25] which, although not specified, is assumed to be for spherical crystals as in a similar study [23]).

To evaluate the change in bulk Gibbs energy, we note that the initial state of the participating ions and water molecules is supersaturated solution, while the final state is pure, hydrated crystal. The chemical potential of the salts is equal across the crystal-solution interface if the solution is saturated. Therefore, assuming water activity approximately equal to one, ΔG_V can be related to the saturation index (SI, defined in [29]):

$$\Delta G_V = RT\ln\left[\frac{\left(a_{\mathrm{Ca}^{2+}} a_{\mathrm{SO_4}^{2-}} a_w^2\right)_{\mathrm{sat}}}{a_{\mathrm{Ca}^{2+}} a_{\mathrm{SO_4}^{2-}} a_w^2}\right]\frac{\rho_x}{M_w} = -\frac{\ln(10)\mathrm{SI}\ RT\rho_x}{M_w} \ , \qquad (10)$$

where R is the universal gas constant, T is the absolute temperature, a is the activity (of single ions or water, subscript w), and the subscript sat corresponds to saturation conditions. The critical radius, $r_{c,}$ is then estimated to be:

$$r_c = \frac{2\gamma M_w}{\ln(10)\ \rho_x RT\ \mathrm{SI}} \ . \qquad (11)$$

2.2 Induction Time

To complete the model, the induction time for crystallization as a function of temperature and concentration is needed. We use a correlation based on gypsum induction time data collected by Alimi and Gadri [30] for calcium sulfate nucleation in solutions mixed from calcium chloride and sodium sulfate (as in this work) with a quartz crystal microbalance. We assume that the actual nucleation period is linearly proportional to the measured induction time, which includes some time for undetected growth. The data used in the correlation span temperatures between 20–70 °C and saturation indices between 0.32–0.64. The fit is based on an empirical relationship recommended by He et al. [23] for the dependence of nucleation time on saturation index (SI) at a given temperature:

$$\log_{10}(t_{ind}) = \frac{b}{\mathrm{SI}^2} - c. \qquad (12)$$

The empirical constant *c* was found to be nearly a linear function of temperature and *b* was considered to be proportional to T^3 in accordance with the nucleation theory described in Ref. [23], neglecting lower-order effects of temperature on growth rate. The following correlation was fit from the Alimi and Gadri data [25] for SI<0.6:

$$\log_{10}(t_{ind}) = \frac{8.511\times10^6}{\mathrm{SI}^2 T^3} - 0.0269T + 10.464. \qquad (13)$$

Figure 3 shows that the correlation (Eq. (13)) fits the data well.

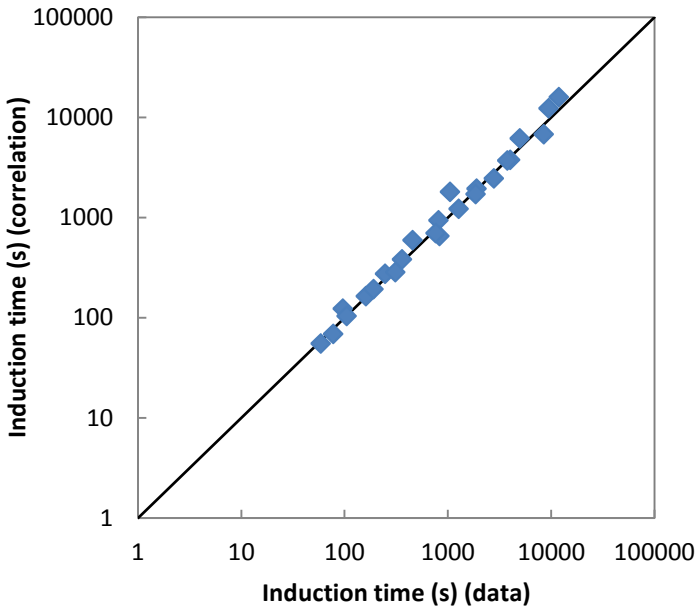

Figure 3. Fit (Eq. (13)) of gypsum induction time data by Alimi and Gadri [25].

Based on the model of residence time and the fit of induction time experimental data, regime maps can be produced by solving $t_{ind}(T, \mathrm{SI}) = \varphi\, t^*_{res}(T, \mathrm{SI}, L, v, h)$ for transition points between regions where fouling will and will not occur. The experiments described in the following section are used to validate this theory.

Values of parameters used in evaluating the model are given in Table 1.

Table 1. Model Parameters

Variable	Symbol	Value
Molecular weight ($CaSO_4{\cdot}2H_2O$)	M_w	0.1722 kg/mol
Crystal density	ρ_x	2360 kg/m^3
Liquid dynamic viscosity (function of temperature)	μ_l	4.3×10^{-4}–6.5×10^{-4} Pa-s
Temperature	T	40–70 °C
Surface energy of the crystal–solution interface	γ	0.048 J/m^2 [25]

3. Experimental Methods

Fouling tests were performed in a membrane distillation system (Fig. 4) with controlled temperature, flow rate, and feed pressure. Calcium sulfate concentration, temperature, and flow rate

were varied to validate the proposed framework for predicting the incidence of fouling in membrane distillation. The apparatus has been previously described, and further details are in references [2] and [6]. The system had a very thin permeate gap, similar to conditions in conductive gap MD [31], a configuration that has higher energy efficiency and permeate flux than other MD configurations [32]. Additional tests were conducted with a modified apparatus in air-gap configuration with a sapphire transparent condensing plate. The flux in these experiments was lower due to the low thermal conductivity of the sapphire plate contributing a significant thermal resistance [33].

Conditions were chosen to represent real MD systems [6]. Reynolds numbers ranged from high laminar to low turbulent conditions, and permeate flux (5-40 kg/m^2-hr), dimensions, and hot-side temperatures (40-70 °C) are comparable to those seen in real systems [8, 9, 10, 34, 35, 36]. Calcium sulfate, one of the two most common salts that foul in membrane distillation, was used as a model foulant under supersaturated conditions. To form supersaturated $CaSO_4$ solutions, two component salts, $CaCl_2$ and Na_2SO_4 (ACS grade, Sigma-Aldrich), were dissolved fully and added one at a time (about 10 minutes apart) to allow for thorough mixing. Before adding foulant, the system was heated to its final temperature at the desired flow rate and pressure and allowed to run salt-free until a steady flux was reached (around 4-8 hours). Trials were run for up to 72 hours, but stopped after fouling was observed, as evidenced by flux decline >5% or by salt rejection dropping below 99% (presumably as a result of pore wetting). In the unfouled state, rejection exceeded 99.9%. The predicted induction time for nucleation is less than 72 hours for all but one of the tests (SI_m=0.2, T_m=50 °C). Several of the trials for which no fouling occurred were run even longer (up to 112 hours) to ensure that the 72 h time period was long enough, but none of the trials that were unfouled at 72 hours experienced fouling after longer run times. Some experiments were repeated to confirm repeatability.

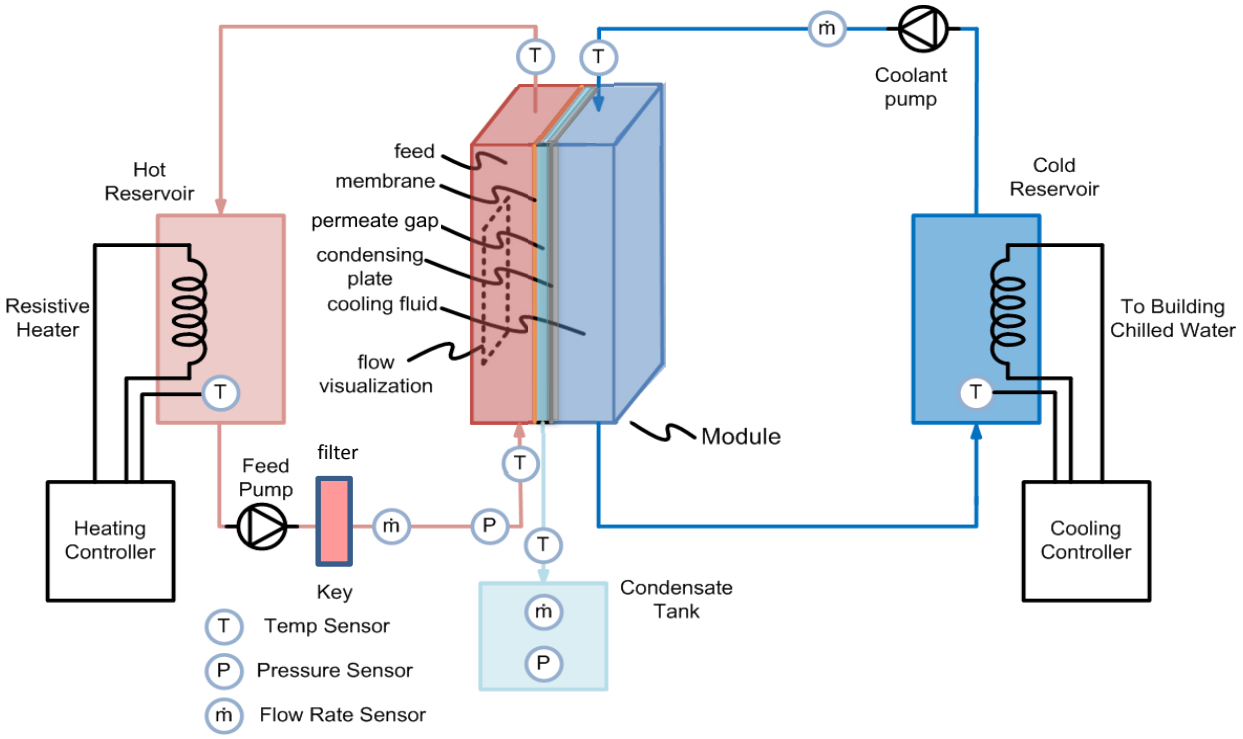

Figure 4. Schematic diagram of the fouling apparatus (figure from [6]). The permeate gap MD module has two flow loops for the hot saline feed and cooling fluid.

The PVDF MD membranes (Millipore ISEQ00010) used in this study are 200 µm thick with a 0.2 µm nominal pore size. The membrane is relatively hydrophobic, with a static contact angle of 125°. Water was filtered with a Pentair pleated cellulose filter with a 20 µm nominal pore size before being introduced to the module to avoid secondary nucleation from any pre-existing crystals. Care was taken to avoid bulk and surface nucleation outside of the module, as should be done in any supersaturated desalination system. No metal or other materials with high surface energy were exposed to the liquid. The heater was enclosed in a thin plastic bag that minimized temperature gradients and prevented the feed fluid from touching the metal heater.

Table 2 provides a summary of the system geometry and operating conditions.

Table 2. Experiment values and uncertainty

Variable	Value	Uncertainty

Feed Channel		
Feed temp	40-70 °C	±0.1°C
Feed flow rate	0.044-0.32 kg/s	±0.003 kg/s
Length	16 cm	±0.1 mm
Width	12 cm	±0.1 mm
Depth	5 mm	±0.1 mm
No-flux entrance length	20.7 cm	±0.1 mm
Feed pressure	0.3 atm	±0.025 atm
Gap		
Thickness (permeate gap)	<0.1 mm	n/a
Thickness (air gap)	0.7-0.8 mm	±0.05 mm
Pressure	1 atm	±0.025 atm
Distillate flux	5-40 kg/m^2-hr	±0.2 kg/m^2-hr
Cooling Channel		
Coolant temp	20 °C	±0.5 °C
Coolant flow rate	0.2 kg/s	±0.003 kg/s

3.1 Modeling of Membrane Conditions

The experiments were paired with a one dimensional discretized numerical model for membrane distillation to calculate concentrations of various ions (Na^+, Cl^-, Ca^{2+}, and SO_4^{2-})and temperature near the membrane surface. These vary from bulk values due to heat and mass transfer resistance offered by the boundary layers . The modeling methodology has been described in detail previously [2, 6, 37], and hence is only briefly discussed here. The membrane condition model has also been previously validated [37].

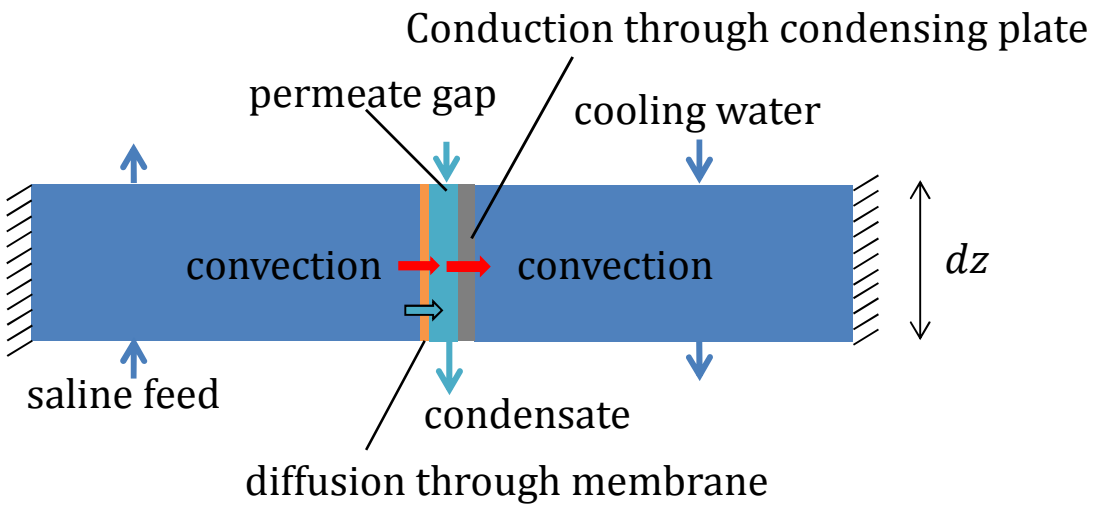

Figure 5. Computational cell for model of heat and mass transfer in membrane distillation [6, 38]

The model, executed using Engineering Equation Solver [39], uses the finite difference method and solves simultaneous equations describing conservation of mass and energy in each computational cell. The model includes heat convection in the hot and cold streams, diffusion through the membranes using the membrane permeability, diffusion through the air gap, and condensation in the permeate gap [40]. The concentration and temperature values in the fluid bulk and near the membrane surface obtained from the model are then used to determine the SI using PHREEQC [41]. The phreeqc.dat database was used, which gives similar results as pitzer.dat database and captures the temperature dependence of solubility of CaSO4 (anhydrite) and CaSO4.2H2O (gypsum) in pure CaSO4 solutions.

4. Results and Discussion

4.1 Fouling Conditions

Fouling was indicated by either flux decline or product salinity increase, both of which are standard methods of fouling detection [5]. Examples are given in Fig. 6.

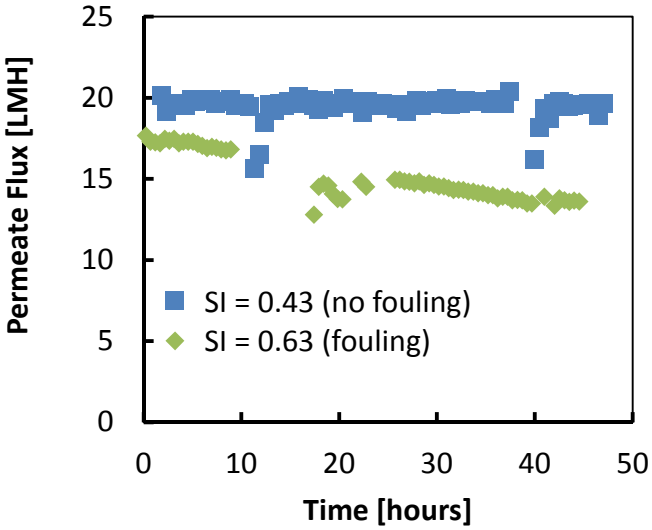

Figure 6. Permeate flux in trials at 66 °C, 0.315 m/s.

While the flux decline and salinity cutoffs for determining the occurrence of fouling required only small changes (≥3% decrease in flux), generally the changes were very apparent (e.g., 20% decrease in flux). As seen in Fig. 6, flux declined 24% for the fouled trial, but remained within the small scale flux fluctuations (±0.5%) for the unfouled test. Slight dips occurred in the data for both: this is a result of the necessity to add more DI water to the tank to replace that which has been desalinated: this reduces the temperature, reducing flux briefly, and requires a brief gap in recording while the permeate is removed from the scale.

Trials in which fouling occurred exhibited crystals on the membrane surface (see, e.g., Fig. 7).

Figure 7. SEM Image of fouled membrane surface, showing what appear to be gypsum crystals, from the experiment with an SI of 0.63 and feed temperature at the membrane of 67°C.

Typically, large crystals (Fig. 7) were observed in a few locations while most of the membrane remained unfouled. Nucleation of the crystals on the membrane itself is not favored due to the low surface energy of hydrophobic MD membranes. More hydrophilic surfaces, such as seen in RO membranes, will likely exhibit significant surface nucleation [19], and thus crystals will be more common and more uniformly distributed [42].

The extended (3-5 day) testing periods were important, as the effects of fouling take time to impact flux and permeate conductivity. For instance, a preliminary trial at 60°C and SI = 0.62 found no evidence fouling until the second day.

4.2 Locating the Most Fouling-Prone Region of the Module

When extending this model to real systems, which have spatially-varying flow rate, temperature, and salinity, the modeling should focus on the region most prone to fouling. We use the one-dimensional heat and mass transfer model [37] (Fig. 5) to map residence and induction times and identify the most fouling-prone region.

For fouling of the main salts of concern, $CaSO_4$ and $CaCO_3$, some conditions make fouling worse at the beginning of the module, while others may exacerbate fouling at the end. As the analysis in this section shows, the beginning of the module is likely to be the most fouling-prone in real MD systems.

At the entrance, temperature is highest, and fouling propensity increases at higher temperatures due to the inverse solubility for both salts [5]. In addition, concentration polarization is worse at this location due to the higher permeate flux [43]. However, at the end of the module, the bulk concentration is higher due to the finite water recovery. In reverse osmosis, this effect is the most significant, leading to more severe scaling at the end of the module due to the higher water recovery compared to MD, and lack of temperature variation [44].

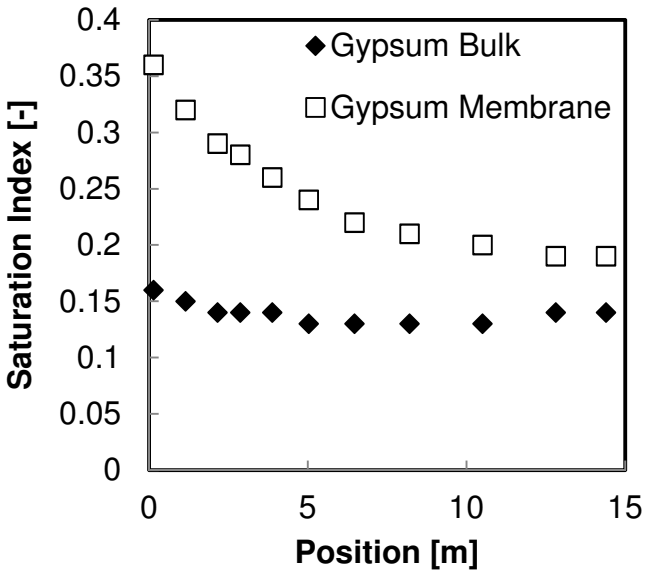

Figure 8. Calculated saturation index of gypsum at the membrane surface and in the feed bulk solution across an MD module of representative industrial length L = 14.4 m, width = 0.5 m, channel depth = 1 mm, and feed velocity = 0.23 m/s [45, 46]. For this system, the bulk temperature at the entrance was 80 °C and dropped to 34 °C at the feed exit. The concentration of $CaSO_4$ in the feed inlet is 2.5 g/kg, and the overall system flux is 4.2 kg/m^2-hr.

To help determine the module region of primary concern, the temperature, flow rate, and SI can be calculated throughout the module to find the induction time everywhere. Using calculated temperature and salinity profiles, the saturation index for $CaSO_4$ can be found at the membrane surface and in the bulk (Fig. 8). The saturation index near the membrane surface is consistently higher than in the feed bulk due to concentration polarization, in spite of the temperature in the feed bulk being higher. The SI of gypsum drops along the module length. Because the induction time decreases at higher SI and higher temperature, the conditions near the entrance region are likely to cause the most rapid nucleation of crystals, as seen in Fig. 9, where induction time is lowest at the entrance and increases rapidly along the length. [44]

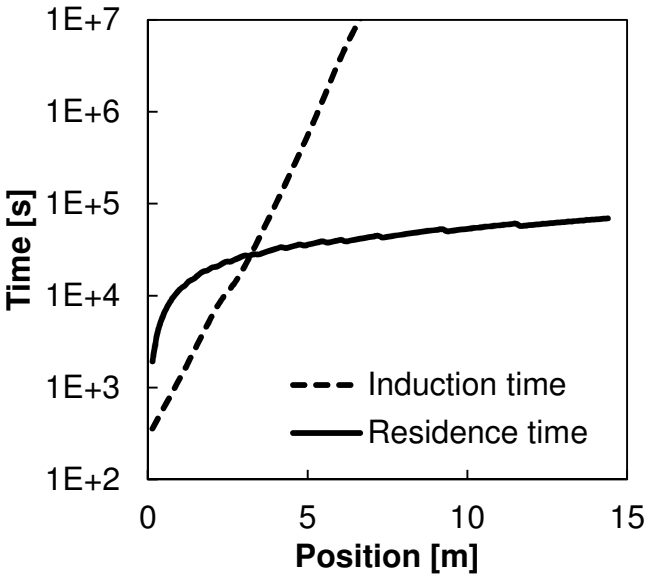

Figure 9. Induction time and residence time along the length of a full-scale MD module with 2.5 g/kg $CaSO_4$ at the inlet. Where residence time exceeds induction time, nucleation and fouling can be expected.

As seen in Fig. 9, residence time increases almost linearly in space, whereas induction time increases more rapidly as the saturation index at the membrane drops along the length of the module. This plot does not consider the experimentally inferred factor φ, which would further reduce the effective residence time, and does not attempt to calculate the residence time at the inlet, where entrance effects are highly dependent on module design. For the conditions considered in Fig. 9, residence time exceeds induction time for positions greater than approximately 0.1 m, and the ratio of residence time to induction time is maximized 1 m from the inlet. Residence time is higher than induction time only in the initial section of the module, where flux is highest, and therefore predicting fouling-free operation using the inlet conditions to predict induction time and outlet conditions to predict residence time is conservative. To be more precise, induction and residence times can be computed throughout the module to look for areas of overlap.

4.3 Experimental Validation of Fouling Model

Experimental gypsum fouling results are reported in Figs. 10 and 11 to demonstrate agreement with the proposed theory and fit the correction factor φ. The fitting parameter that best matched all experimental data was φ=0.15. The overlap of the non-fouling trial at 66 °C and SI=0.43 with the theoretical threshold is not necessarily cause for concern, as the saturation index did tend to fall slightly over time in the high temperature experiments (which have shorter induction times) due to crystallization in the tank and filter; this has been accounted for in the experimental uncertainty. [47]

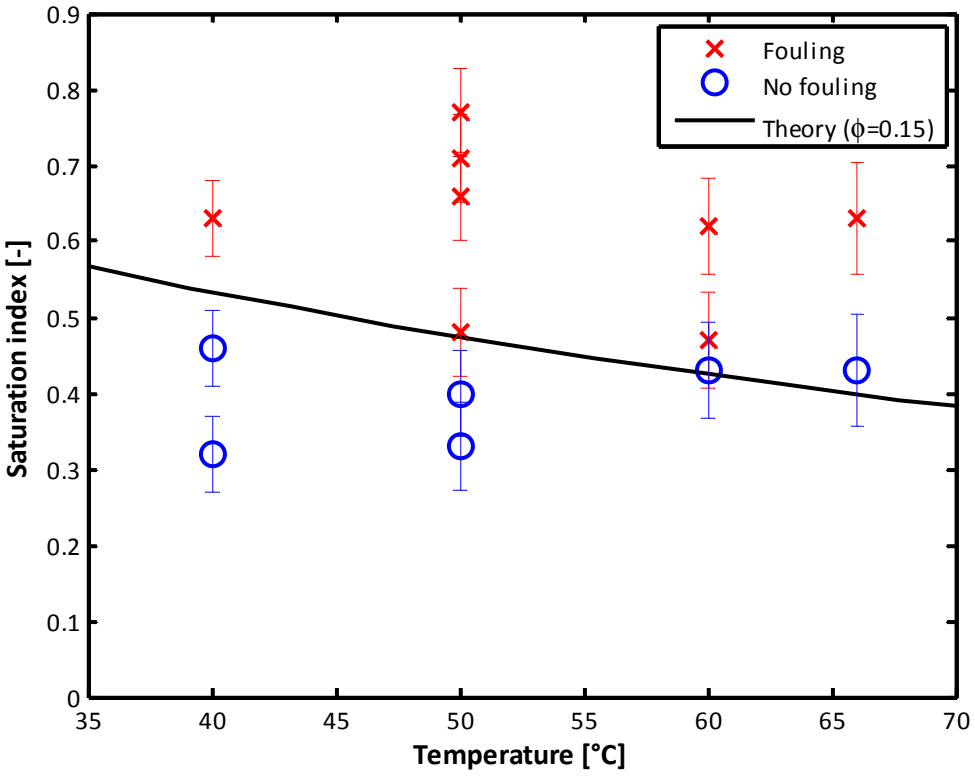

Figure 10. Experimental fouling regime map overlaid with the theoretical prediction for $CaSO_4$ at varied temperature and salinity at a single flow rate (0.314 m/s). Permeate flux varied from 7.5-30 kg/m^2-hr as temperature increased.

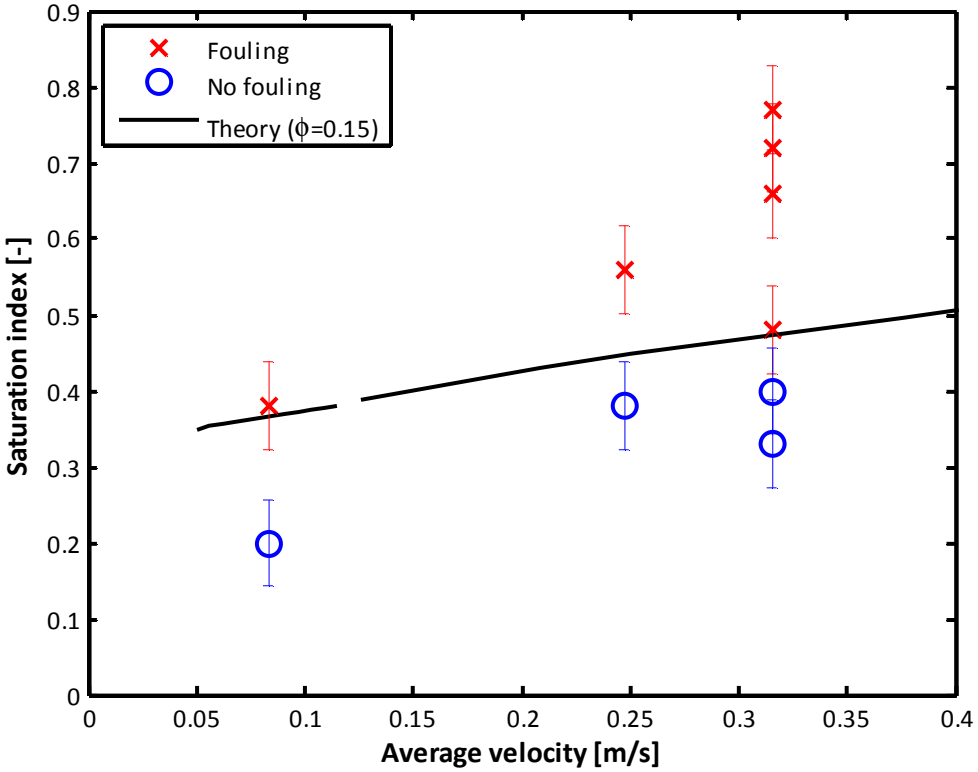

Figure 11. Experimental fouling regime map overlaid with the theoretical prediction for $CaSO_4$ at 50 °C and three feed velocities. The break in the theoretical threshold represents the transition region between laminar and turbulent flow in the channel. Permeate flux varied from 18.0-19.2 kg/m^2-hr for the tests at 0.08 and 0.32 m/s and about 8 kg/m^2-hr for the tests at feed velocity of 0.24 m/s where a transparent sapphire condensing surface with lower thermal conductivity was used.

In Fig. 12, all measurements taken during this study are combined with measurements made using a different MD module[2] [47, 48] to show the level of agreement between model predictions and measurements across varying temperatures, velocities, and channel dimensions. In addition to the data shown in Figs. 10 and 11, Fig. 12 includes an additional measurement at 40 °C and 27 cm/s flow rate. For each data point, the actual SI is plotted against the maximum SI without fouling that would be

[2] In the experiments of Tow et al., the same membrane was used in a module of 8 cm length, 3 cm width, and 1 mm depth at a cross-flow velocity of 5 cm/s and a feed-side average membrane temperature of 58.5 °C. See [47, 48] for more information. Calcium sulfate solutions were filtered for 36 hours or until fouling (marked by 20% decline in flux) was apparent.

predicted based on the conditions of the trial. Ideally, the positive fouling results would be above the 1:1 line and negative fouling results would be below it. In fact, most points do fall on the correct side, and the few that fall on the wrong side are within their experimental uncertainty of the line.

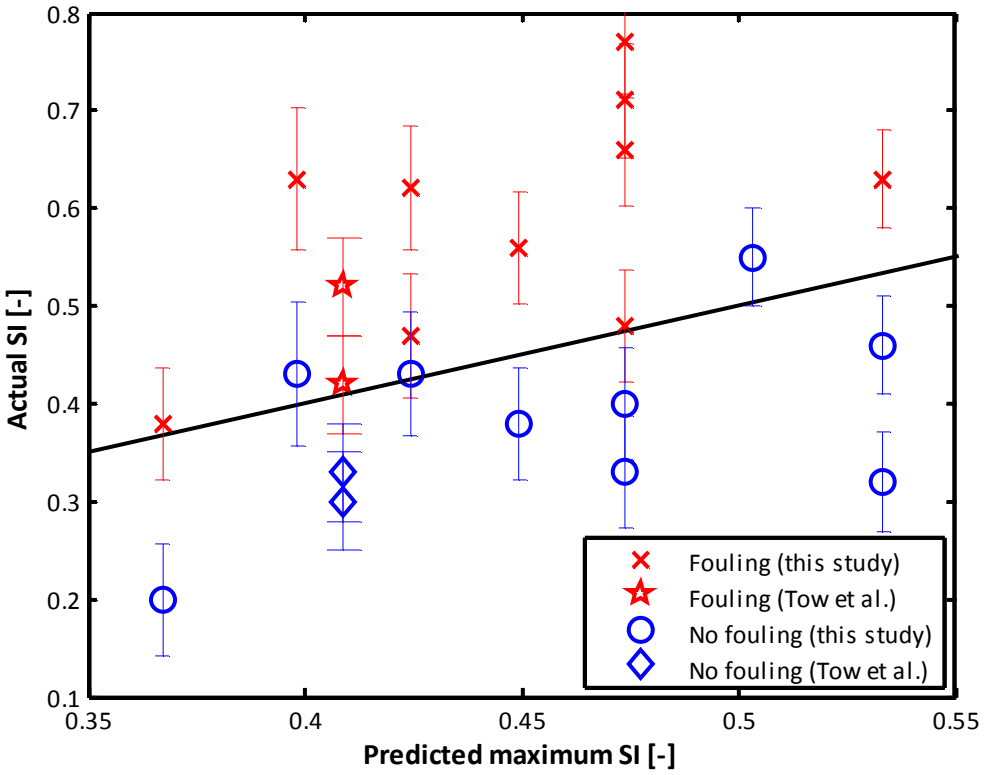

Figure 12. Validation of model using all present measurements plus data collected from a different MD module by Tow et al. [48].

The experimental results support the use of the proposed model to bound safe operating conditions for a range of MD systems at risk of gypsum scaling. Although it is not very precise, it provides an upper bound on acceptable supersaturation, which expands the range of operating conditions beyond saturation conditions. Future work is needed to show whether the same theoretical approach can predict fouling with other scalants such as calcium carbonate.

4.4 Theoretical $CaSO_4$ Fouling Regime Maps

The proposed methodology reduces the complex problem of scaling prediction to three primary variables (membrane SI and temperature, and the flow parameter $L/f_d v^2$) to allow for simple prediction of fouling in almost any MD system. Because the residence time is a function of SI, T, and the ratio $L/f_d v^2$ and the induction time is only a function of SI and T, the condition for fouling ($t_{ind} \leq \varphi t_{res}$*) can be plotted with only three variables (Fig. 13) using φ=0.15. For ease of use, the same map was plotted in terms of $CaSO_4$ concentration in Fig. 14. The transition between laminar and turbulent flow that appears as a gap in Fig. 11 is captured by the Darcy friction factor, and thus there is no gap or discontinuity in the regime maps that follow.

The present theory can be extended across a range of operating conditions to create a universal regime map for scaling prediction, demonstrated here for $CaSO_4$ (Figs. 13 and 14). To use these maps, the $CaSO_4$ saturation index (with Fig. 13) or concentration (with Fig. 14) at the membrane must be supplied along with the temperature near the membrane, module length, bulk velocity, feed channel depth, and fluid kinematic viscosity. First, calculate Reynolds number of the flow and the Darcy friction factor f_d using Eqns. (7) and (8). Next, compute the term $L/(f_d v^2)$ and locate the correct position on the abscissa. If the point ($L/(f_d v^2)$, SI) in Fig. 13 or ($L/(f_d v^2)$, C) in Fig. 14 is below the line corresponding to the temperature at the membrane, fouling is unlikely. Operation above the line for a given temperature should be avoided. Operating conditions falling close to the line should be approached with care, as there is some uncertainty associated with these maps and they have not yet been validated with complex feeds or in large-scale systems.

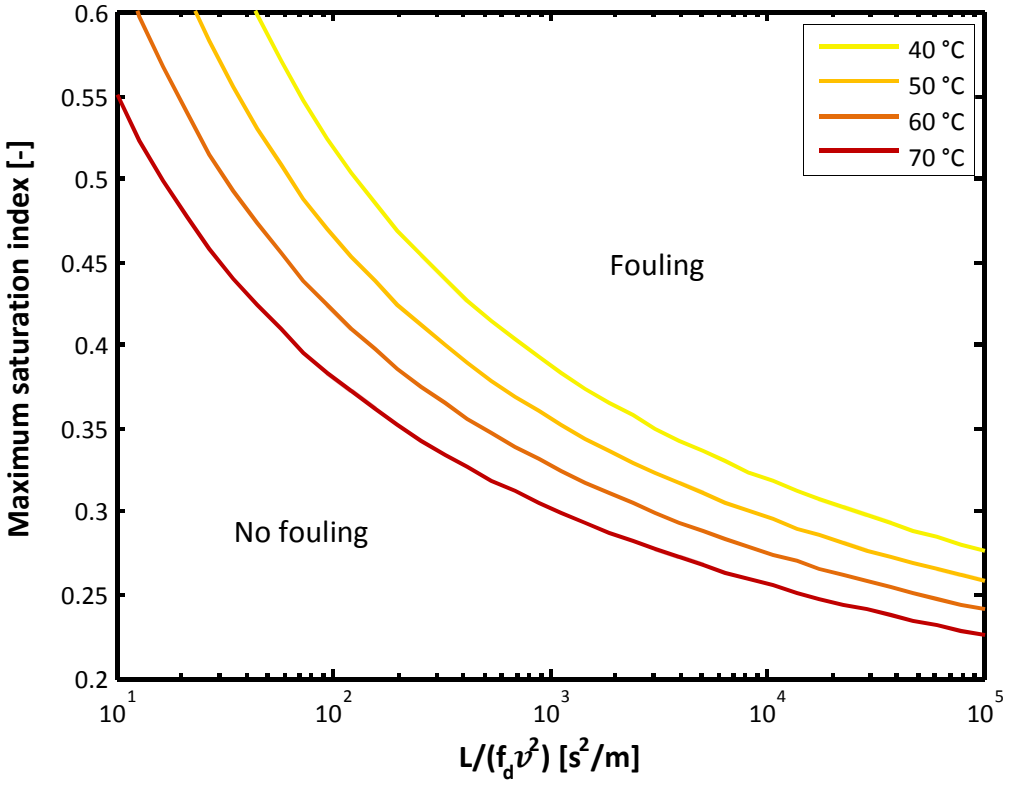

Figure 13. Universal $CaSO_4$ fouling regime map: at saturation indices above the curve for a given temperature, systems are prone to fouling according to the present model. The horizontal axis incorporates membrane length *L*, Darcy friction factor f_d, and bulk velocity *v*. The incorporation of f_d collapses laminar and turbulent flow regimes into the same curve.

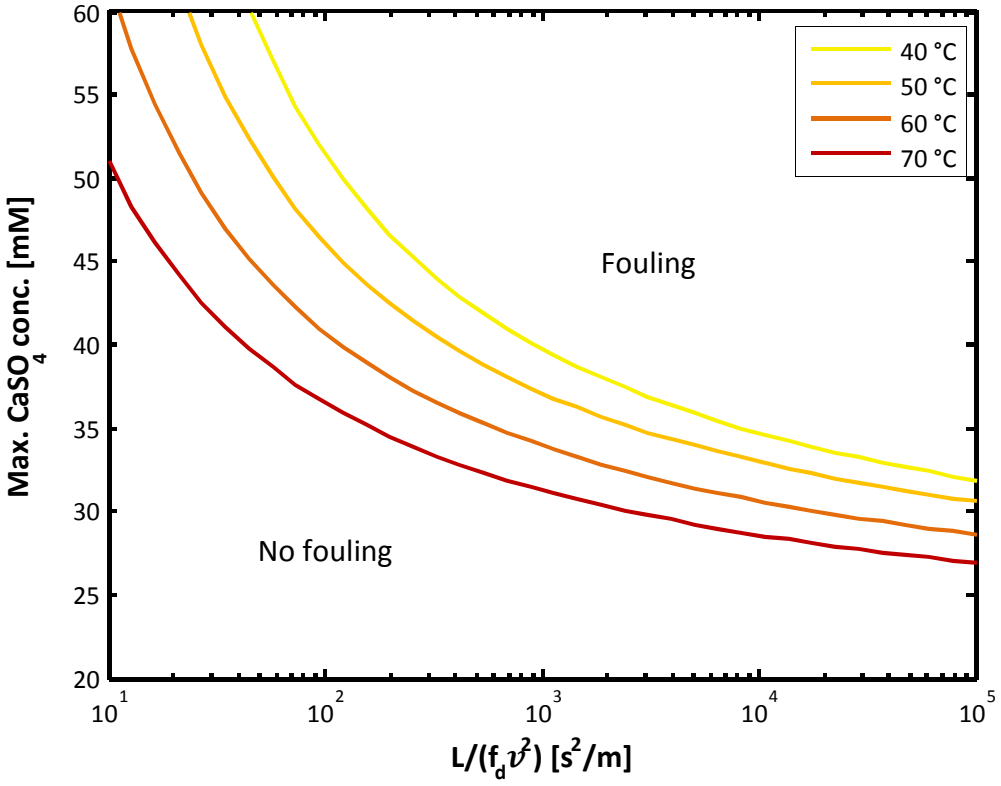

Figure 14. Universal CaSO4 fouling regime map given in terms of concentration: at concentrations above the curve for a given temperature, systems are prone to fouling according to the present model.

Because temperature and concentration (or SI) are evaluated at the membrane surface, this methodology requires calculating temperature and concentration polarization. The heat and mass transfer model of Ref. [37] can be used, or the wall temperature and concentration can be estimated with reasonable accuracy using correlations for fully developed internal flow in a channel [49], neglecting permeate flux through the membrane.

The regime maps identify two primary trends that can inform fouling-resistant MD system design. First, a larger residence time parameter, $L/f_d v^2$, leads to a decrease in the maximum allowable SI. Higher temperatures also lead to a decrease in maximum allowable SI due to the shorter induction times at high temperatures. In general, long membranes and low cross-flow velocities should be avoided, and high temperatures should be used with caution.

4.5 Implications for MD System Design

In real systems, induction times may vary as a result of complex feed solutions including particulate matter, which may accelerate nucleation, or antiscalants, which aim to prevent nucleation. To account for such variations, induction times can be experimentally tested using practices applied in antiscalant testing [50] to determine tolerable operating conditions.

The present study showed that the strongest predictor of fouling (other than scalant concentration) is feed velocity. Although the effect of spacers was not modeled, the demonstrated effect of residence time on fouling implies that spacer design can play a role in fouling prevention. Spacers can also reduce the increase in SI between the bulk solution and the membrane region by reducing concentration polarization. On the other hand, poor spacer designs that create dead zones have the potential to intensify fouling through effects of both concentration polarization and residence time.

Finally, high surface energy surfaces such as metal walls or less hydrophobic membranes should be avoided because they may encourage surface nucleation where the solution is supersaturated. The ability of MD systems to operate above saturation relies on the long induction time due to the high energy barrier to bulk nucleation, and high-energy surfaces may provide favorable nucleation sites and reduce the concentration at which scaling occurs.

5. Conclusion

Theory was developed to predict the incidence of scaling in MD by deriving a relevant residence time and equating it to induction time. Crystal nucleation is predicted to occur in the bulk fluid near the membrane, where the highest concentrations and longest residence times occur. This approach to scaling prediction was validated against experimental results with calcium sulfate over a range of temperatures, saturation indices, and fluid velocities.

The model shows that MD systems can be operated under supersaturated conditions without fouling if the nucleation induction time is sufficiently long. Regime maps based on the model (Figs. 13 and 14) are generated to simplify the selection of safe operating conditions for a wide range of MD systems with varying temperatures, flow rates, and dimensions.

Acknowledgement

This work was funded by the Cooperative Agreement between the Masdar Institute of Science and Technology, Abu Dhabi, UAE and the Massachusetts Institute of Technology (MIT), Cambridge, MA, USA, Reference no. 02/MI/MI/CP/11/07633/GEN/G/00. EWT acknowledges that this material is based upon work supported by the National Science Foundation Graduate Research Fellowship Program under Grant No. 1122374 and the MIT Martin Fellowship for Sustainability. We would like to thank Prof Allan Myerson, Luke Roberto, McCall Huston, Tamanna Urmi, Margaret Bertoni, Maria Rosa Ruiz, and Hyung Won Chung for their contributions to this work.

Appendix A: Additional Modeling Results

To clarify the relationship between bulk and near-membrane fluid properties, the heat and mass transfer model is solved over a length of membrane to show lengthwise variation in temperature (Fig. 15) and salinity (Fig. 16).

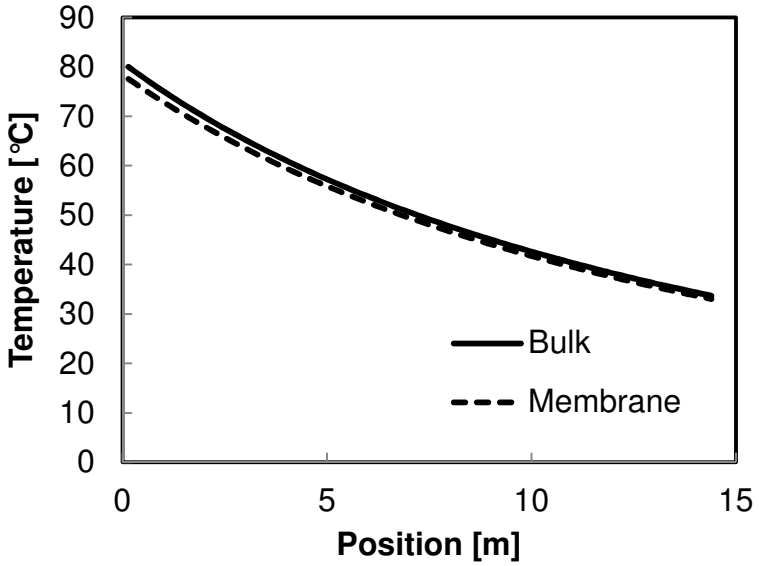

Figure 15. Modeled feed temperature profiles across a long MD module.

As seen in Fig. 15, the temperature declines as it passes through the module. Temperature polarization, which causes the difference between bulk and near-membrane temperature, can be

manipulated by modifying the Nusselt number. The Nusselt number may be increased by changing the flow rate or channel depth or by using spacers to enhance turbulence, particularly spacers of high thermal conductivity.

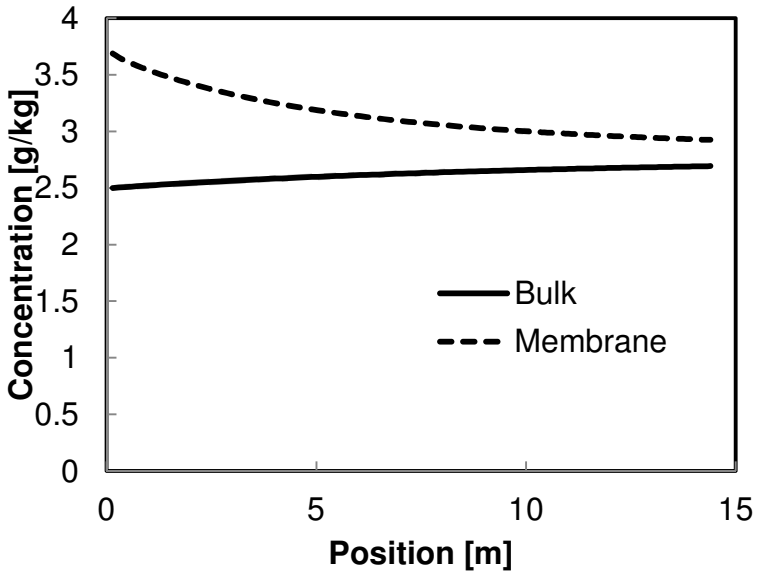

Figure 16. Modeled $CaSO_4$ concentration profiles across a long MD module.

As seen in Fig. 16, concentration in the feed channel increases as pure waterleaves through the membrane. On the other hand, near-membrane concentration is higher near the channel inlet where concentration polarization is maximum due to a much higher pure water flux.

Appendix B: Implications for Brine Recirculation

Brine recirculation (Fig. 17) is often used in MD concentration applications because single-stage MD systems typically have low recovery on the order of 5-10% [31, 51]. Secondary nucleation leads to rapid crystallization in MD, and systems that retain and recirculate the feed indefinitely (i.e., brine recirculation), cannot operate above saturation without inevitable scaling. However, multistage or batch systems that filter out crystals in between stages or cycles may reduce scaling by discouraging secondary nucleation.

In this study, concerns about the effect of recirculation on residence time were avoided by cleaning the system before the start of every trial, initiating data collection as soon as salts were added to the feed tank, filtering the feed before every pass, avoiding excessive temperature gradients in the feed tank, and using sufficiently high fluxes such that concentration polarization was significant and nucleation induction times were much shorter in the module than in the recirculation tank.

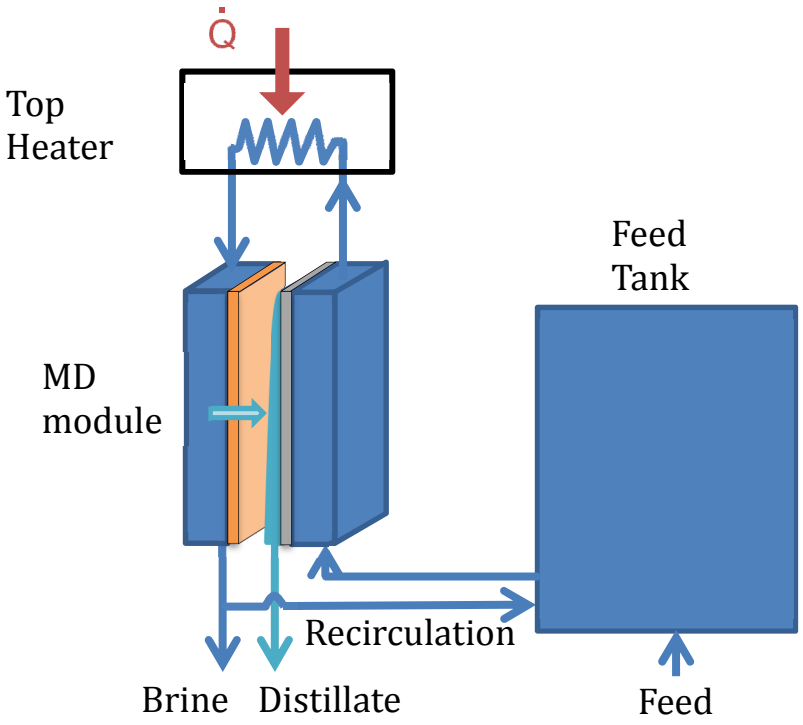

Figure 17. Schematic diagram of membrane distillation with brine recirculation.

References

[1] C. Cabassud and D. Wirth, "Membrane distillation for water desalination: How to choose an appropriate membrane?" *Desalination*, vol. 157, no. 1-3, pp. 307–314, 2003. [Online]. Available: http://linkinghub.elsevier.com/retrieve/pii/-S0011916403004107

[2] D. M. Warsinger, J. Swaminathan, and J. H. Lienhard V, "Effect of module inclination angle on air gap membrane distillation," in *Proceedings of the 15th International Heat Transfer Conference, IHTC-15, Paper No. IHTC15-9351*, Kyoto, Japan August 2014. [Online]. Available: http://web.mit.edu/lienhard/www/papers/conf/IHTC15-9351_Warsinger.pdf

[3] H. W. Chung, J. Swaminathan, D. Warsinger, and J. H. Lienhard V, "Multistage vacuum membrane distillation (MSVMD) system for high salinity application," *Journal of Membrane Science*, vol. 497, pp. 128–141, 2016.

[4] M. M. Pendergast and E. M. Hoek, "A review of water treatment membrane nanotechnologies," *Energy & Environmental Science*, vol. 4, no. 6, pp. 1946–1971, 2011.

[5] D. M. Warsinger, J. Swaminathan, E. Guillen-Burrieza, H. A. Arafat, and J. H. Lienhard V, "Scaling and fouling in membrane distillation for desalination applications: A review," *Desalination*, vol. 356, pp. 294–313, 15 Jan. 2015. Available: http://www.sciencedirect.com/science/article/pii/S0011916414003634

[6] D. M. Warsinger, J. Swaminathan, , H. W. Chung, S. Jeong, and J. H. Lienhard V, "The effect of filtration and particulate fouling in membrane distillation," in *Proceedings of The International Desalination Association World Congress on Desalination and Water Reuse, San Diego, CA, USA, IDAWC15- Warsinger-51667*, Aug 2015. [Online]. Available: http://-hdl.handle.net/1721.1/100445

[7] F. He, J. Gilron, H. Lee, L. Song, and K. K. Sirkar, "Potential for scaling by sparingly soluble salts in crossflow DCMD," *Journal of Membrane Science*, vol. 311, no. 1-2, pp. 68–80, 2008. [Online]. Available: http://linkinghub.elsevier.com/-retrieve/pii/S0376738807008393

[8] N. Dow, S. Gray, J. Zhang, E. Ostarcevic, A. Liubinas, P. Atherton, G. Roeszler, A. Gibbs, M. Duke *et al.*, "Pilot trial of membrane distillation driven by low grade waste heat: Membrane fouling and energy assessment," *Desalination*, vol. 391, pp. 30–42, 2016.

[9] H. C. Duong, S. Gray, M. Duke, T. Y. Cath, and L. D. Nghiem, "Scaling control during membrane distillation of coal seam gas reverse osmosis brine," *Journal of Membrane Science*, vol. 493, pp. 673–682, 2015.

[10] E. Guillen-Burrieza, A. Ruiz-Aguirre, G. Zaragoza, and H. A. Arafat, "Membrane fouling and cleaning in long term plant-scale membrane distillation operations," *Journal of Membrane Science*, vol. 468, pp. 360–372, 2014.

[11] S. Shirazi, C.-J. Lin, and D. Chen, "Inorganic fouling of pressure-driven membrane processes – A critical review," *Desalination*, vol. 250, no. 1, pp. 236–248, 2010. [Online]. Available: http://linkinghub.elsevier.com/retrieve/pii/-S0011916409007541

[12] V. Calabro, B. L. Jiao, and E. Drioli, "Theoretical and experimental study on membrane distillation in the concentration of orange juice," *Industrial & Engineering Chemistry Research*, vol. 33, no. 7, pp. 1803–1808, 1994.

[13] E. Drioli, Y. Wu, and V. Calabro, "Membrane distillation in the treatment of aqueous solutions," *Journal of Membrane Science*, vol. 33, no. 3, pp. 277–284, 1987.

[14] K. Lawson and D. Lloyd, "Membrane distillation," *Journal of Membrane Science*, vol. 124, no. 1, pp. 1–25, 1997. [Online]. Available: http://linkinghub.elsevier.com/retrieve/pii/S0376738896002360

[15] T. Van Gassel and K. Schneider, "An energy-efficient membrane distillation process," *Membranes and Membrane Processes*, pp. 343–348, 1986.

[16] K. Karakulski, M. Gryta, and A. Morawski, "Membrane processes used for potable water quality improvement," *Desalination*, vol. 145, no. 1-3, pp. 315–319, 2002. [Online]. Available: http://linkinghub.elsevier.com/retrieve/pii/-S0011916402004290

[17] G. Meindersma, C. Guijt, and A. de Haan, "Desalination and water recycling by air gap membrane distillation," *Desalination*, vol. 187, no. 1-3, pp. 291–301, 2006. [Online]. Available: http://linkinghub.elsevier.com/retrieve/pii/-S0011916406000087

[18] E. Guillen-Burrieza, R. Thomas, B. Mansoor, D. Johnson, N. Hilal, and H. A. Arafat, "Effect of dry-out on the fouling of PVDF and PTFE membranes under conditions simulating intermittent seawater membrane distillation (SWMD)," *Journal of Membrane Science*, vol. 438, pp. 126–139, 2013. [Online]. Available: http://linkinghub.elsevier.com/-retrieve/pii/S0376738813002093

[19] D. M. Warsinger, A. Servi, S.Van Belleghem, J. Gonzalez, J. Swaminathan, J. Kharraz, H. W. Chung, H. A. Arafat, K. K. Gleason, J. H. Lienhard V, "Combining air recharging and membrane superhydrophobicity for fouling prevention in membrane distillation," *Journal of Membrane Science*, vol. 505, pp. 241–252, 2016.

[20] E. Curcio, E. Fontananova, G. Di Profio, and E. Drioli, "Influence of the structural properties of poly(vinylidene fluoride) membranes on the heterogeneous nucleation rate of protein crystals," *The Journal of Physical Chemistry B*, vol. 110, no. 25, pp. 12438–12445, 2006.

[21] E. Curcio, X. Ji, G. Di Profio, A. O. Sulaiman, E. Fontananova, and E. Drioli, "Membrane distillation operated at high seawater concentration factors: Role of the membrane on $CaCO_3$ scaling in presence of humic acid," *Journal of Membrane Science*, vol. 346, no. 2, pp. 263–269, 2010. [Online]. Available: http://linkinghub.elsevier.com/retrieve/pii/-S0376738809007017

[22] D. Cohen-Tanugi, R. K. McGovern, S. H. Dave, J. H. Lienhard, and J. C. Grossman, "Quantifying the potential of ultra-permeable membranes for water desalination," *Energy & Environmental Science*, vol. 7, no. 3, pp. 1134–1141, 2014.

[23] S. He, J. E. Oddo, and M. B. Tomson, "The nucleation kinetics of calcium sulfate dihydrate in NaCl solutions up to 6 M and 90 °C," *Journal of Colloid and Interface Science*, vol. 162, no. 2, pp. 297–303, 1994.

[24] A. G. Xyla, J. Mikroyannidis, and P. G. Koutsoukos, "The inhibition of calcium carbonate precipitation in aqueous media by organophosphorus compounds," *Journal of Colloid and Interface Science*, vol. 153, no. 2, pp. 537–551, 1992. [Online]. Available: http://www.sciencedirect.com/science/article/pii/002197979290344L

[25] F. Alimi and A. Gadri, "Kinetics and morphology of formed gypsum," *Desalination*, vol. 166, pp. 427 – 434, 2004. [Online]. Available: http://www.sciencedirect.com/science/article/pii/S001191640400325X

[26] M. Çelikbilek, A. E. Ersundu, and S. Aydn, *Crystallization Kinetics of Amorphous Materials*. INTECH Open Access Publisher, 2012.

[27] F. M. White, *Fluid Mechanics, 6th edition*. New York, NY: McGraw Hill, 2006.

[28] F. M. White and I. Corfield, *Viscous fluid flow, 3rd edition*. McGraw-Hill New York, 2011.

[29] G. P. Thiel and J. H. L. V, "Treating produced water from hydraulic fracturing: Composition effects on scale formation and desalination system selection," *Desalination*, vol. 346, pp. 54 – 69, 2014. [Online]. Available: http://-www.sciencedirect.com/science/article/pii/S0011916414002574

[30] F. Ahmi and A. Gadri, "Kinetics and morphology of formed gypsum," *Desalination*, vol. 166, pp. 427–434, 2004.

[31] J. Swaminathan, H. W. Chung, D. M. Warsinger, F. A. Al-Marzooqi, A. H. Arafat, and J. H. Lienhard V, "Energy efficiency of permeate gap and novel conductive gap membrane distillation," *Journal of Membrane Science*, vol. 502, pp. 171–178, 2016.

[32] J. Swaminathan, H. W. Chung, D. M. Warsinger, and J. H. Lienhard V, "Membrane distillation model based on heat exchanger theory and module comparison," *Submitted to Applied Energy, November 2015*, 2015.

[33] L. L. Morales, "Visualization and measurement of filmwise and dropwise air gap membrane distillation at varied module inclination angle and gap spacer orientation," Ph.D. dissertation, Massachusetts Institute of Technology, 2016.

[34] E. Guillén-Burrieza, J. Blanco, G. Zaragoza, D.-C. Alarcón, P. Palenzuela, M. Ibarra, and W. Gernjak, "Experimental analysis of an air gap membrane distillation solar desalination pilot system," *Journal of Membrane Science*, vol. 379, no. 1-2, pp. 386–396, 2011. [Online]. Available: http://linkinghub.elsevier.com/retrieve/pii/S0376738811004479

[35] E. Guillén-Burrieza, G. Zaragoza, S. Miralles-Cuevas, and J. Blanco, "Experimental evaluation of two pilot-scale membrane distillation modules used for solar desalination," *Journal of Membrane Science*, vol. 409-410, pp. 264–275, 2012. [Online]. Available: http://linkinghub.elsevier.com/retrieve/pii/S0376738812002645

[36] E. K. Summers and J. H. Lienhard V, "A novel solar-driven air gap membrane distillation system," *Desalination and Water Treatment*, vol. 51, pp. 1344–1351, 2013. [Online]. Available: http://www.tandfonline.com/doi/abs/10.1080/19443994.2012.705096

[37] E. K. Summers, H. A. Arafat, and J. H. Lienhard V, "Energy efficiency comparison of single-stage membrane distillation (MD) desalination cycles in different configurations," *Desalination*, vol. 290, pp. 54–66, 2012. [Online]. Available: http://linkinghub.elsevier.com/retrieve/pii/S0011916412000264

[38] D. Warsinger, "Thermodynamic design and fouling of membrane distillation systems," Ph.D. dissertation, Massachusetts Institute of Technology, 2015. [Online]. Available: https://dspace.mit.edu/handle/1721.1/100154

[39] S.A.Klein, "Engineering equation solver version 9," *F-Chart Software*.

[40] D. M. Warsinger, J. Swaminathan, L. Maswadeh, and J. H. Lienhard V, "Superhydrophobic condenser surfaces for air gap membrane distillation," *Journal of Membrane Science*, vol. 492, pp. 578–587, 2015.

[41] D. L. Parkhurst and C. Appelo, "Description of input and examples for phreeqc version 3â€"a computer program for speciation, batch-reaction, one-dimensional transport, and inverse geochemical calculations," *US geological survey techniques and methods, book*, vol. 6, p. 497, 2013.

[42] G. Azimi, Y. Cui, A. Sabanska, and K. K. Varanasi, "Scale-resistant surfaces: Fundamental studies of the effect of surface energy on reducing scale formation," *Applied Surface Science*, vol. 313, pp. 591–599, 2014.

[43] A. Alkhudhiri, N. Darwish, and N. Hilal, "Membrane distillation: A comprehensive review," *Desalination*, vol. 287, pp. 2–18, 2012. [Online]. Available: http://linkinghub.elsevier.com/retrieve/pii/S0011916411007284

[44] M. T. Khan, M. Busch, V. G. Molina, A.-H. Emwas, C. Aubry, and J.-P. Croue, "How different is the composition of the fouling layer of wastewater reuse and seawater desalination RO membranes?" *Water Research*, vol. 59, no. 0, pp. 271 – 282, 2014. [Online]. Available: http://www.sciencedirect.com/science/article/pii/S0043135414003030

[45] H. C. Duong, P. Cooper, B. Nelemans, T. Y. Cath, and L. D. Nghiem, "Evaluating energy consumption of air gap membrane distillation for seawater desalination at pilot scale level," *Separation and Purification Technology*, vol. 166, pp. 55 – 62, 2016. [Online]. Available: http://www.sciencedirect.com/science/article/pii/S1383586616301897

[46] A. Jansen, J. Hanemaaijer, J. Assink, E. Sonsbeek, C. Dotremont, and J. Medevoort, "Pilot plants prove feasibility of a new desalination technique," *Asian Water*, vol. 26, pp. 22–26, 2010.

[47] D. M. Warsinger, E. W. Tow, and J. H. Lienhard V, "Inorganic fouling resistance of membrane distillation vs. reverse osmosis," in *Proceedings of Singapore Water Week 2016 (SIWW), Singapore*, July 2016.

[48] E. W. Tow, D. E. M. Warsinger, J. Swaminathan, A. M. Trueworthy, G. P. Thiel, S. M. Zubair, A. S. Myerson, and J. H. Lienhard V, "Comparison of fouling propensity between membrane distillation and reverse osmosis," *In preparation*, 2016.

[49] J. H. Lienhard IV and J. H. Lienhard V, *A Heat Transfer Textbook, Fourth Edition*. Phlogiston Press, 2016. [online] http://ahtt.mit.edu

[50] F. He, K. K. Sirkar, and J. Gilron, "Effects of antiscalants to mitigate membrane scaling by direct contact membrane distillation," *Journal of Membrane Science*, vol. 345, no. 1-2, pp. 53–58, 2009. [Online]. Available: http://-linkinghub.elsevier.com/retrieve/pii/S0376738809006085

[51] D. M. Warsinger, K. H. Mistry, K. G. Nayar, H. W. Chung, and J. H. Lienhard V, "Entropy generation of desalination powered by variable temperature waste heat," *Entropy*, vol. 17, pp. 7530–7566, 2015.